

Measuring cosmic rays with the LOFAR radio telescope

**K. Mulrey,^{b,e,*} S. Buitink,^{a,b} A. Corstanje,^{a,b} M. Desmet,^a H. Falcke,^{b,d,e}
B. M. Hare,^d J. R. Hörandel,^{a,b,e} T. Huege,^{a,f} V. B. Jhansi,^c N. Karastathis,^f
G. K. Krampah,^a P. Mitra,^a B. Neijzen,^d A. Nelles,^{g,h} H. Pandya,^a O. Scholten,^{i,j}
K. Terveer,^h S. Thoudam,^c G. Trinh^k and S. ter Veen^d**

^aVrije Universiteit Brussel, Astrophysical Institute, Pleinlaan 2, 1050 Brussels, Belgium

^bDepartment of Astrophysics/IMAPP, Radboud University Nijmegen, P.O. Box 9010, 6500 GL Nijmegen, The Netherlands

^cDepartment of Physics, Khalifa University, P.O. Box 127788, Abu Dhabi, United Arab Emirates

^dNetherlands Institute for Radio Astronomy (ASTRON), Postbus 2, 7990 AA Dwingeloo, The Netherlands

^eNikhef, Science Park Amsterdam, 1098 XG Amsterdam, The Netherlands

^fInstitut für Astroteilchenphysik, Karlsruhe Institute of Technology (KIT), P.O. Box 3640, 76021 Karlsruhe, Germany

^gDeutsches Elektronen-Synchrotron DESY, Platanenallee 6, 15738 Zeuthen, Germany

^hECAP, Friedrich-Alexander-Universität Erlangen-Nürnberg, 91058 Erlangen, Germany

ⁱInteruniversity Institute for High-Energy, Vrije Universiteit Brussel, Pleinlaan 2, 1050 Brussels, Belgium

^jUniversity of Groningen, Kapteyn Astronomical Institute, Groningen, 9747 AD, Netherlands

^kDepartment of Physics, School of Education, Can Tho University Campus II, 3/2 Street, Ninh Kieu District, Can Tho City, Vietnam

E-mail: k.mulrey@astro.ru.nl

The LOFAR radio telescope has been used to measure radio emission from cosmic-ray air showers in the $10^{16} - 10^{18}$ eV range for over a decade. LOFAR's uniquely dense array of hundreds of antennas measuring from 30-80 MHz is ideal for probing the radio footprint in detail. To date, LOFAR data have been used to reconstruct cosmic ray energy, arrival direction, and depth of shower maximum with an average precision better than 20 g/cm^2 . LOFAR is currently undergoing an upgrade (LOFAR 2.0) which will enable continuous observation and a tenfold increase in data rate, as well as a wider measurement bandwidth. We have recently doubled the size of the particle detector triggering array located at LOFAR to maximize the benefits of this upgrade. We are also developing new analysis techniques in order to best utilize the new influx of data. In this contribution, we present an overview of the detector, recent results, and future plans for cosmic ray detection with the LOFAR radio telescope.

38th International Cosmic Ray Conference (ICRC2023)
26 July - 3 August, 2023
Nagoya, Japan



*Speaker

1. The LOFAR telescope

LOFAR (Low Frequency Array) is the world's largest radio telescope, consisting of antenna stations distributed across northern Europe and a dense core of 24 stations in the Netherlands [1]. Each LOFAR station consists of two sets of 48 dual-polarized Low Band Antennas (LBAs) that operate in the 30 – 80 MHz band as well as High Band Antennas (HBAs) which operate between 120 – 240 MHz. LOFAR serves primarily as a telescope for radio astronomy, however, it can also be used to measure radio emission from cosmic-ray air showers. This is facilitated by the LORA particle detector array, which consists of 40 plastic scintillators, and is also situated at the LOFAR core [2]. LORA detects air showers between 10^{16} – 10^{18} eV and acts as a trigger to readout the buffered data from each antenna. This energy range is scientifically interesting because it is the region where the origin of cosmic rays is expected to shift from galactic to extragalactic sources.

LOFAR makes an ideal experiment for measuring the radio emission generated in cosmic-ray air showers, which is predominantly generated by the geomagnetically induced, time-varying transverse current that develops as the shower propagates through the atmosphere [3]. The resulting radio “footprint” provides a calorimetric energy measurement and is sensitive to the shower development, meaning it can be used to reconstruct features of the air shower such as the position of X_{\max} . The dense antenna spacing in the core makes LOFAR unique among radio detection experiments, and the detailed LOFAR measurements helped establish the technique of detecting air showers via radio emission. In this contribution, we present an overview of current LOFAR cosmic-ray analyses, methods to expand the scope of what simulations are possible, and plans for the LOFAR 2.0 upgrade, which will take place in the coming years.

2. Recent results

2.1 Mass composition

Results for cosmic-ray composition as determined using LOFAR data, which demonstrated for the first time that radio measurements could be used to determine X_{\max} , were presented in 2016 [4, 5]. This analysis was based on CORSIKA [6] and CoREAS [7] simulations. Particle data measured by LORA was used to set the energy scale, as no absolute calibration for the radio data had yet been implemented. Since then, an absolute calibration has been developed using the Galactic background and a model of the LOFAR signal chain to predict the background levels expected in the data [8]. This makes it possible to do fully radio-based analyses, without relying on information from the particle detectors. Additionally, the X_{\max} analysis relies on having accurate simulations, with realistic atmospheric conditions at the time of any event. To accommodate this, a tool was developed to include time-dependent and location-specific atmospheric models directly in CoREAS simulations [9]. An updated composition analysis in the $10^{16.8}$ – $10^{18.3}$ eV range was presented in 2021, including these improvements, as well as increased event statistics and improved anti-bias cuts [10] (see Figure 1). The results were consistent with a significant light-mass fraction of 23 – 39 % protons and helium (depending on the choice of hadronic interaction model) and with the fraction of intermediate-mass nuclei dominating. This is consistent with earlier LOFAR results, but now with the systematic uncertainties on X_{\max} lowered to 7 – 9 g/cm².

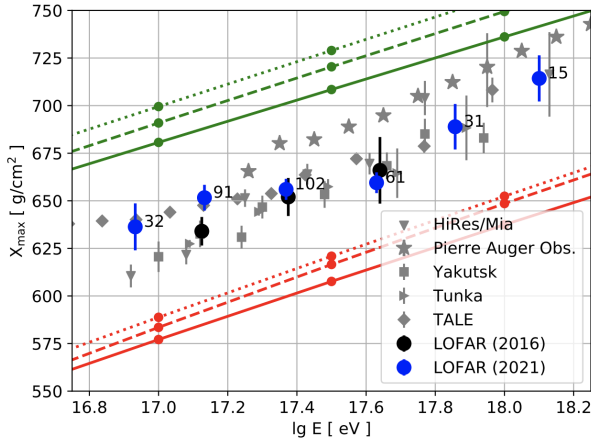


Figure 1: The average depth of X_{\max} , as a function of primary particle energy [10]. The annotated numbers indicate the number of showers in each bin. The error margins indicate the uncertainty on the mean of the X_{\max} distribution. The upper lines indicate the mean values expected for protons, from simulations with QGSJetII-04 (solid), EPOS-LHC (dashed) and Sibyll-2.3d (dotted). The lower lines show the mean predicted values for iron nuclei. Results from Pierre Auger [11], Yakutsk [12], Tunka [13], HiRes/Mia [14], and TALE [15] are also shown.

It is worth noting that, while the results of LOFAR and the Pierre Auger Observatory agree within statistical and systematic uncertainties, we do find a slightly lower average X_{\max} . LOFAR values are in tension with those found at Pierre Auger Observatory, but they agree with results from other experiments in the Northern hemisphere. A similar analysis using radio data has been performed at the Auger Engineering Radio Array (AERA) [16], and found X_{\max} results consistent with Auger fluorescence measurements [17]. There is an active working group between people involved in both of these analyses to try and understand the difference.

2.2 X_{\max} reconstruction with MGMR3D

Typical LOFAR analyses are heavily based on Monte Carlo simulations done using CORSIKA and CoREAS [6, 7]. This has the advantage that the simulations capture the natural shower-to-shower fluctuations that occur in nature. Furthermore, the radio footprint produced by CoREAS has been shown to reproduce data extremely well. The disadvantage to this approach, however, is that these simulations are computationally expensive, with computational times scaling with the number of antennas simulated. MGMR3D [18] is a fast, semi-analytic code that calculates the complete radio footprint (intensity, polarization, and pulse shapes) using the 3-dimensional structure of an extensive air shower. It can be used to investigate the sensitivity of the radio footprint to shower parameters, like shower width and X_{\max} . These parameters can also be fit using a chi-square optimization with measured radio data. To demonstrate the effectiveness of this technique, selected LOFAR data have been reconstructed with MGMR3D, obtaining a resolution of 22 g/cm² on X_{\max} and an energy resolution of 19% [19]. These results, as well as a sample event reconstructed using both methods, are shown in Figure 2. Although this method does not reach the same resolution on X_{\max} and energy as the CoREAS method, it provides a fast and efficient tool to reconstruct air-shower parameters. It can also be combined with Monte Carlo simulations as a preliminary estimate to help reduce the required simulation time.

2.3 Using pulse-shape information for reconstructing cosmic-ray air showers

As demonstrated above, X_{\max} can be reconstructed on an event-to-event basis using the total energy in the measured signal. However, there is more information contained in the radio signal than

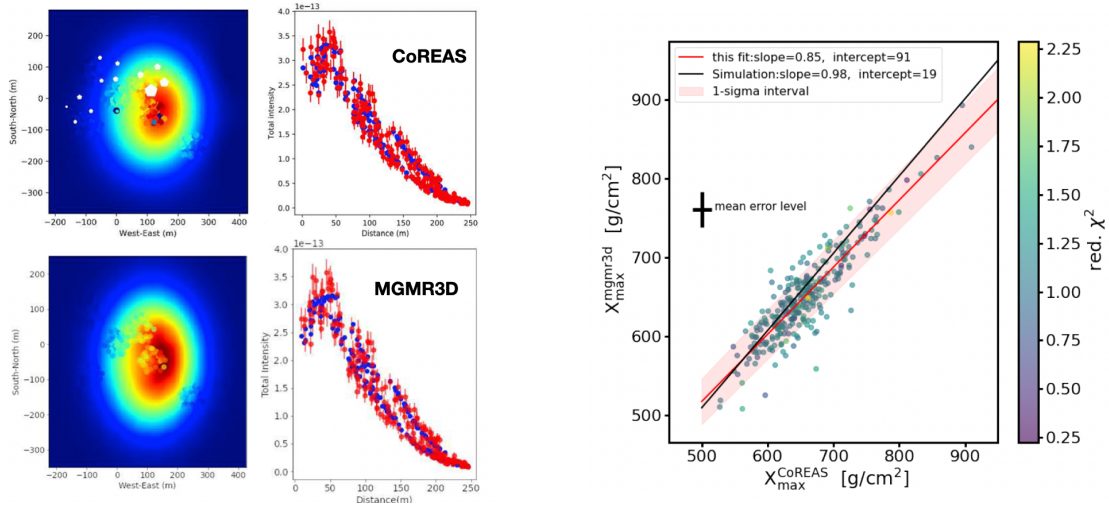


Figure 2: Left: Example of a measured shower fitted with CoREAS (top panel) and MGMR3D (bottom). The plots on the left show the antenna placement on the ground with color-coded measured intensity. The best-fitting simulated footprints with CoREAS and MGMR3D are shown in the background. The one-dimensional LDF intensity profile for each is also shown. Right: Reconstructed X_{\max} of LOFAR events using MGMR3D and CoREAS. The red line is the fit to the data points. The shaded area is the $1\text{-}\sigma$ interval of the fit.

the energy alone. The signal pulse shape contains information both about the distance of the antenna to the shower core, and also subtler information about the shower development. By exploiting the extra information in the pulse shape, it is possible to reconstruct X_{\max} without using information about the signal strength. An example of this is shown in the left panel of Figure 3. The frequency spectrum of an antenna at a given distance from the shower core is shown in yellow. The spectrum from an antenna at the same distance to the core, but for a CoREAS simulation with a different X_{\max} is shown in red. The cumulative amount of fluence as a function of frequency is shown in the right panel, with the total fluence in each pulse normalized to one. The cumulative fluence distributions show a clear difference, which can be quantified by calculating the area between the two distributions. By looking at the combined differences in pulse shape for all the antennas in an event, and comparing this to many simulations with different X_{\max} values, one can identify the simulation that most closely resembles the measured event. This technique works best with signals of larger bandwidth, where differences in pulse shapes are more pronounced, making it an appealing option for future analyses with cosmic rays measured with LOFAR 2.0 and the Square Kilometer Array [20]. For more information about this method, see 2023 ICRC contribution [21].

3. Efforts to address simulation challenges

As mentioned above in the context of MGMR3D, simulations for radio emission from air showers is computationally expensive. Here, we discuss a few methods developed to mitigate this problem.

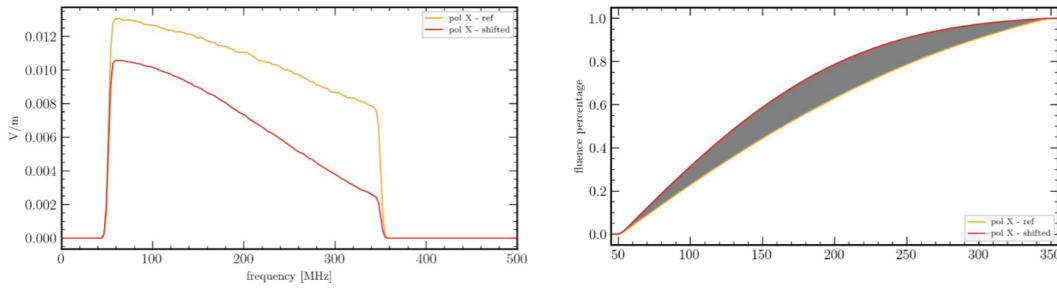


Figure 3: Left: Frequency spectra for two antennas at the same position in the radio footprint, for events with different X_{\max} . Right: The cumulative difference in fluence from each signal, normalized to one at 350 MHz. [Figure to be updated.](#)

3.1 High-order interpolation

Simulations for LOFAR analyses are typically done for antennas in the “star-shaped” pattern, with radial arms of antennas evenly spaced in the $\vec{v} \times \vec{B}$, $\vec{v} \times \vec{v} \times \vec{B}$ plane. Using this design, the fluence at any antenna position in the radio footprint can be interpolated, making use of the radial symmetry of the footprint. This makes it possible to find the fluence at particular LOFAR antenna positions for events with different core positions, using the same simulation. X_{\max} analyses in the 30 – 80 MHz bandwidth have used this approach to save computation time and allow for flexibility in fitting the core position. However, with the prospect of measuring at higher frequencies where there is more structure in the footprint (with LOFAR 2.0 and SKA), and also using the pulse shape information in analyses, we need a new approach to simulation, allowing for the full electric-field pulse to quickly be determined at any given position in the footprint.

This challenge has been addressed by using a higher-order algorithm which interpolates the amplitude and phase spectra of signals in the frequency domain using a Fourier method. The details of this method are given in [22] and also presented at this conference [23]. Figure 4 demonstrates the power of this technique. An example radio fluence footprint of 30 – 500 MHz is shown in the left panel, along with the antenna positions that were fully simulated using CoREAS. 250 additional antennas were simulated at random positions in the shower footprint. This allows for the “true” electric field at these antenna positions to be compared with the field found using the interpolation method. The relative error in interpolated amplitude as a function of total fluence in the pulse is shown in the right panel of Figure 4. Even for very weak signals, the relative error is on the level of a few percent. The relative error is similar for the total energy fluence in the interpolated signal. The code for this interpolation method can be found on github¹.

3.2 Template Synthesis Method

Another approach to managing the simulation challenge is the Template Synthesis Method [24]. This method allows the user to “synthesize” radio emission from an air shower with an arbitrary longitudinal profile from the full Monte Carlo simulation of another shower with the same geometry. The method uses semi-analytical relations which depend on X_{\max} and the desired antenna position, and which were derived by slicing the atmosphere into layers of constant atmospheric depth and

¹<https://github.com/nu-radio/cr-pulse-interpolator>

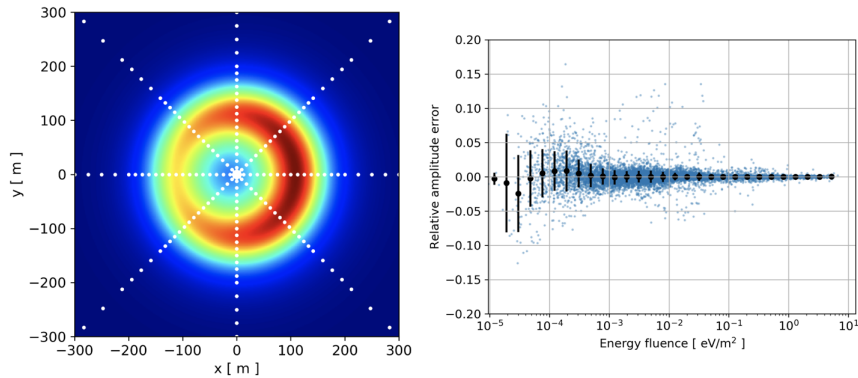


Figure 4: Left: sample simulated footprint using the classic star-shaped pattern. Simulated antenna positions are in white, and interpolated fluence is depicted by the color scale. Right: the relative interpolation error in the amplitude of the signal. Each dot represents a test antenna in one shower of a test ensemble of events. Black dots show the binned mean, and their error bars show the standard deviation.

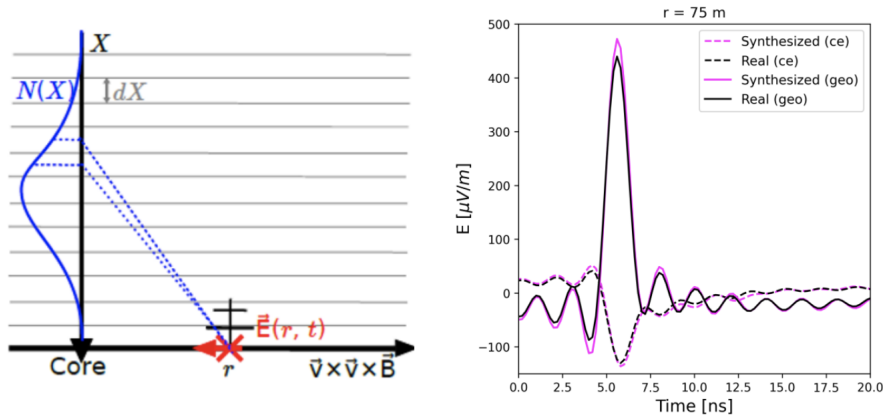


Figure 5: Left: Diagram of how the atmosphere is sliced for the Template Synthesis Method. The radiation from each slice is found using one Monte Carlo simulation, and then scaled appropriately for the desired longitudinal profile. Right: An example of a pulse that has been synthesized using the method.

analyzing the contribution to the total signal in an antenna from each slice. This method has previously been shown to work well for vertical showers, and now the potential for synthesizing radio emission from showers with inclined geometries has been demonstrated. A schematic of how the Template Synthesis Method works is shown in the left panel of Figure 5, and an example of a pulse that has been synthesized is shown in the right panel. For more details about the method, see 2023 ICRC contribution [25].

4. LOFAR 2.0

The LOFAR telescope is currently undergoing a suite of upgrades that will result in LOFAR 2.0. Upgrades include new electronic boards which will improve processing power at the stations, improved clock synchronicity between stations, and software that will allow for multiple antenna

sets to be used at the same time. The work we have done to expand the LORA array and the features of LOFAR 2.0 will offer major improvements to cosmic-ray measurements in the coming years:

- In 2019 the LORA triggering array was doubled in size. This will both allow us to detect more events at high energies, and reduce detection biases at low energies, effectively increasing our measurement energy range [26].
- Currently, cosmic-ray observations primarily make use of the “LBA outer” antenna set. These are used for astronomy observations only a fraction of the time. The software that will allow concurrent observations from multiple antenna sets will offer a factor of 10 increased observation time.
- The HBA antenna sets have not been heavily used in cosmic-ray observations so far because they are beam-formed during observations, and most cosmic-rays don’t arrive with optimal geometry to be observed. In LOFAR 2.0, HBA observations will not be pre-beam formed, which means the raw voltage traces can be used for cosmic-ray observations. This, plus the fact that LBA and HBA observations will happen simultaneously, means that we will be able to do broadband cosmic-ray observations, between 30 – 240 MHz with LOFAR 2.0. This will allow us to explore more features of air-shower development.
- We are in the process of developing an algorithm to monitor the raw stream of radio data from each antenna. Applying finite impulse response filters, we can remove radio frequency interference and also use radio data as part of the cosmic-ray trigger, in conjunction with the particle data. This will have the effect of reducing our energy threshold for triggering, and increasing the number of events we trigger on with a usable cosmic-ray signal.

5. Conclusions

LOFAR has been used to measure radio emission from air showers for over a decade, resulting in detailed analyses of cosmic-ray composition in the Galactic to extragalactic transition region. Now, as we look forward to the next decade of LOFAR 2.0 observations, we are preparing the tools to fully benefit from the increased event rate and extra bandwidth that will be provided. This includes new analysis methods using more information in the pulse shape, as well as advanced simulation techniques to allow us to do these studies. With this, we will be able to continue exploring radio emission from air showers in unprecedented detail.

Acknowledgements

BMH is supported by ERC Grant agreement No. 101041097; AN and KT acknowledge the Verbundforschung of the German Ministry for Education and Research (BMBF). NK acknowledges funding by the Deutsche Forschungsgemeinschaft (DFG, German Research Foundation) – Projektnummer 445154105. MD is supported by the Flemish Foundation for Scientific Research (grant number G0D2621N). ST acknowledges funding from the Abu Dhabi Award for Research Excellence (AARE19-224).

References

- [1] M. P. van Haarlem *et al.* *Astronomy and Astrophysics* **556** (2013) 56.
- [2] S. Thoudam *et al.* *Nucl.Instrum.Meth* **A767** (2014) 339–346.
- [3] K. Werner and O. Scholten *Astropart. Phys.* **29** (2008) 393–411.
- [4] S. Buitink *et al.* *Phys. Rev. D* **90** no. 8, (2014) .
- [5] S. Buitink *et al.* *Nature* **531** no. 7592, (3, 2016) 70–84.
- [6] D. Heck *et al.* *Report FZKA* **6019** (1998) .
- [7] T. Huege, M. Ludwig, and C. W. James *AIP Conf. Proc.* **1535** (2013) 128.
- [8] K. Mulrey *et al.* *Astropart. Phys.* **111** (2019) 1–11.
- [9] P. Mitra *et al.* *Astropart. Phys.* **123** (2020) 102470.
- [10] A. Corstanje *et al.* *Proceedings of the 35th ICRC, Madison, Wisconsin ICRC2019* (2019) .
- [11] G. Mezek *EPJ Web Conf.* **191** (2018) 08008.
- [12] S. Knurenko, I. Petrov, Z. Petrov, and I. Slepsov *PoS ICRC2015* (2016) 254.
- [13] V. V. Prosin *et al.* *EPJ Web Conf.* **99** (2015) 04002.
- [14] Fly’s Eye Collaboration, C. C. H. Jui *AIP Conf. Proc.* **1367** no. 1, (2011) 7–10.
- [15] Telescope Array Collaboration, R. U. Abbasi *et al.* *Astrophys. J.* **865** no. 1, (2018) 74.
- [16] Pierre Auger Collaboration, J. Schulz *PoS ICRC2015* (2016) 615.
- [17] Pierre Auger Collaboration, B. Pont *EPJ Web Conf.* **283** (2023) 02010.
- [18] O. Scholten, G. Trinh, K. D. de Vries, and B. Hare *EPJ Web Conf.* **216** (2019) 03003.
- [19] P. Mitra *et al.* *arXiv:2307.04242* (2023) .
- [20] S. Buitink *et al.* *Proceedings of the 37th ICRC, Nagoya, Japan PoS(ICRC2023)* (2023) .
- [21] N. Karastathis *et al.* *Proceedings of the 37th ICRC, Nagoya, Japan PoS(ICRC2023)* (2023) .
- [22] A. Corstanje *et al.* *Submitted to JINST* (2023) .
- [23] A. Corstanje *et al.* *Proceedings of the 37th ICRC, Nagoya, Japan PoS(ICRC2023)* (2023) .
- [24] M. Desmet *et al.* *arXiv:2307.02939* (2023) .
- [25] M. Desmet *et al.* *Proceedings of the 37th ICRC, Nagoya, Japan PoS(ICRC2023)* (2023) .
- [26] K. Mulrey *et al.* *Proceedings of the 35th ICRC, Madison, Wisconsin PoS(ICRC2019)* (2019) .